

# Shadow of rotating black holes on a standard background screen

S.V.Repin<sup>1</sup>, D.A.Kompaneets<sup>1</sup>, I.D.Novikov<sup>1,2,3</sup>, and V.A.Mityagina<sup>4,5</sup>

<sup>1</sup> Astro Space Center, Lebedev Physical Institute of RAS, 84/32, Profsoyuznaya str., 117997, Moscow, Russia

<sup>2</sup> The Niels Bohr International Academy, The Niels Bohr Institute, Blegdamsvej 17, DK-2100, Copenhagen, Denmark

<sup>3</sup> National Research Center Kurchatov Institute, 1, Kurchatova sq., 123182, Moscow, Russia

<sup>4</sup> Information Technology Lyceum, No.1533, 16, Lomonosovsky av., Moscow, Russia  
e-mail: [info@lit.msu.ru](mailto:info@lit.msu.ru)

<sup>5</sup> Moscow State University, GSP-1, Leninskie Gory, 119991, Moscow, Russia

February 14, 2018

## ABSTRACT

We present the shape of the black hole shadow on the standard background screen as it is registered by the distant observer. The screen is an infinite plane, emitting the quanta uniformly distributed to a hemisphere. The source of emission is considered to be optically thin and optically thick. It is shown that the shape of a black hole shadow depends crucially on the angle between the plane and the view line to the distant observer. The shadow shapes for the different values of this angle are also presented. Both Schwarzschild and Kerr metrics are considered.

**Key words.** Black hole physics; Gravitational lensing: strong; Methods: numerical

## 1. Introduction

Black holes are the most intriguing objects in astrophysics. Their existence was predicted by the General theory of Relativity (GR). However, the radii of black holes appear to be so small that they cannot be observed immediately yet. Usually, observers register the effects in the accretion disks surrounding the black holes, but not the black holes themselves. One possible way to observe black holes (at least theoretically!) is to observe their shadows.

The black hole shadow is the area in the celestial sphere around the black hole position from which no one quanta comes to the observer. The size of this area does not coincide with the size of the event horizon. The aim of this paper is to consider the structure of the shadow in addition to the many considerations performed earlier (Amarilla & Eiroa 2015; Ghasemi-Nodehi et al. 2015; Neronov & Vovk 2016; Abdujabbarov et al. 2016; Cunha et al. 2016; Shipley & Dolan 2016). The largest angular size is the black hole shadow in the center of our Galaxy and it is approximately 54 micro arc seconds in diameter (Gillessen et al. 2009) under the assumption that the black hole is described by the Schwarzschild metric and the standard background screen is perpendicular to the view line. The second largest is the elliptic galaxy M87 ( $\theta \approx 22$  to 41 micro arc seconds (Walsh et al. 2013)) and the third is the Andromeda galaxy M31 ( $\theta \approx 14$  to 30 micro arc seconds (Bender et al. 2005)). It is evident that the objects of the microsecond size can be observed in detail and investigated only by the interferometers because the angular resolution of the radiotelescopes is much lower.

The Event Horizon Telescope (EHT) could be one of these instruments (Akiyama et al. 2015) as well as Millimetron in Russia (Kardashev et al. 2014) and GRAVITY in Chile (Lacour et al. 2014; Vincent, Paumard & Perrin 2014).

The shape of a black hole shadow depends on the objects and the matter that presents in the vicinity of the black hole. The image of the black hole shadows in M87 (Dexter, McKinney & Agol 2012; Moscibrodzka et al. 2016) and Sgr A\* (Broderick et al. 2016; Johannsen et al. 2016) have been simulated many times under the different assumptions. The simulations take into account the jet and the accretion disk, the effects of hydrodynamics, magnetic fields, optical depth of the disk and a lot of other effects. As a result, these simulations can give a detailed image of a particular object, but cannot reveal the effect of pure lensing. But sometimes, the general view is necessary. So, it would be interesting to demonstrate the effects of General Relativity only, i.e. to present a shadow of a black hole on the sample background of a very simple structure like a bright infinite plane (we will call it a standard screen) and reveal the details of the image, which can be directly observed and which will indicate that the object is definitely the black hole.

In this paper we present the shape of a black hole shadow and the distribution of the emission intensity in the vicinity of the edge on the background of a standard screen as it is registered by the distant observer. The other model of the emission of the standard screen will be considered at the end of Section 6.

## 2. Geometry

We should consider a black hole that is placed in front of a bright plane, which is infinitely far from the observer. We will consider the different inclination of the standard screen to the view line. The observer should also be at infinity with respect to both the black hole and the bright plane. However, these assumptions are very inconvenient for the computations and it would be desirable to avoid the infinite values of variables. Therefore, we should place our objects at the finite distances, but, except for the black hole, they should be outside the area of strong gravity. That is the model we accept.

Let the standard screen (a bright plane) is perpendicular to the  $x$ -axis and crosses this axis at the coordinate  $x_0 = -1000 r_g$ , where  $r_g = 2Gm/c^2$ . It means that the equation of this plane is  $x = -1000 r_g$  ( $y$  and  $z$  can have arbitrary values). Later we will consider the change of the angle between the plane and the  $x$ -axis. The observer is also on the  $x$ -axis, but her coordinates are:  $(1000 r_g, 0, 0)$ . The black hole is located in the center of the Cartesian system, so its coordinates are:  $(0, 0, 0)$ . This design means that both the standard screen and the observer are in the non-relativistic region, where classical mechanics approximations can be applied successfully. The region of strong gravitation, where the General relativity should be counted, surrounds the center of the coordinate system.

When we change the inclination of the standard screen (with respect to the view line) we assume that the distance between the screen and the black hole remains unchanged and equals to  $1000 r_g$ . The same geometry is used when we consider the spinning black hole.

## 3. Simulation methods

To build the shadow of the black hole we need to simulate the trajectories of the huge amount of quanta, emitted uniformly by a standard screen in a solid angle  $2\pi$  and select only those, which are registered by (comes to) the distant observer. This is a direct way, but it requires an extremely long computation time because much of the quanta have to be discarded. Because of that, it is preferable to simulate the quanta propagation in opposite direction, i.e. from the observer to the standard screen. Thus, we count the quanta which are registered by the observer only and avoid the calculation of the trajectories which pass by him. This method, however, can be applied to the Schwarzschild black holes, but not to the spinning ones, because the ray reversibility principal is not satisfied in the Kerr metric. But this difficulty can be overcome by changing the direction of rotation of the black hole to the opposite one.

So, one should consider the trajectories of the quanta, which start from the observer and move to the black hole so that the maximum value of their impact parameter would be 3-4 times higher than the value at which the quanta are captured by the black hole. It corresponds to the impact parameter of approximately  $8 \div 10 r_g$ .

The standard screen is considered to be optically thin, so its brightness is a constant.

The equations of motion for the quantum can be reduced to the system of six ordinary differential equations

(Zakharov 1994; Zakharov & Repin 1999, 2002):

$$\frac{dt}{d\sigma} = -a (a \sin^2 \theta - \xi) + \frac{r^2 + a^2}{\Delta} (r^2 + a^2 - \xi a), \quad (1)$$

$$\frac{dr}{d\sigma} = r_1, \quad (2)$$

$$\frac{dr_1}{d\sigma} = 2r^3 + (a^2 - \xi^2 - \eta) r + (a - \xi)^2 + \eta, \quad (3)$$

$$\frac{d\theta}{d\sigma} = \theta_1, \quad (4)$$

$$\frac{d\theta_1}{d\sigma} = \cos \theta \left( \frac{\xi^2}{\sin^3 \theta} - a^2 \sin \theta \right), \quad (5)$$

$$\frac{d\phi}{d\sigma} = - \left( a - \frac{\xi}{\sin^2 \theta} \right) + \frac{a}{\Delta} (R^2 + a^2 - \xi a), \quad (6)$$

where  $t, 1/r, \theta, \phi$  are the Boyer – Lindquist coordinates,  $\eta = Q/M^2 E^2$  and  $\xi = L_z/ME$  – the Chandrasekhar constants,  $Q$  – the Carter constant (Carter 1968),  $E$  – the quantum energy at the infinity,  $L_z$  – the projection of the momentum of the quantum to  $z$ -axis,  $\sigma$  – the independent variable,  $\Delta = r^2 - 2/r + a^2$ . The auxiliary variables  $r_1$  and  $\theta_1$  do not have adequate physical sense, they are necessary to relieve the computational problems only.

The system (1)-(6) has been solved numerically by the program package, which applies the combination of Gear (Gear 1971) and Adams methods and is distributed freely in Internet (Petzold 1983).

## 4. Trajectories

We take into consideration all the trajectories, which start on the standard screen and come to the distant observer (the direction of the propagation we've discussed above). The vast majority of the photons arrive at the observer after the deviation in the field of a black hole at the angle from 0 to 90 degrees. These rays form the outer bright ring around the shadow of a black hole; it is a kind of radiance or a crown. The impact parameter of the quanta here is greater than approximately  $3.1 r_g$  in Schwarzschild metric. In other words, the value of the impact parameter separates the shadow from the outer bright area. In Kerr metric, the situation is asymmetric and depends on the direction of the black hole rotation.

There is some quanta that performs a few revolutions (one or more) around the black hole before they arriving at the observer. These quanta form a thin annulus inside the shadow area. The structure of this annulus we will discuss below.

The top panels in Fig. 1 demonstrate the flat trajectories in Schwarzschild (left) and extreme Kerr (right) fields, respectively. Both panels demonstrate: (a) the trajectories with the same impact parameter that pass on either sides (right and left) of the black hole; (b) the trajectories, which turn by  $90^\circ$  angle from their initial direction of propagation; (c) the trajectories which turn by  $270^\circ$  angle ( $3/4$  of the full revolution). The quanta of (b) section correspond to the border between the exterior bright area and the area of the shadow. The quanta of (c) section separate the dark area of the shadow and outer edge of the bright annulus inside the shadow. In Kerr metric the left and right trajectories are asymmetric because one of the quanta flies in the same direction as the spinning of the black hole (and

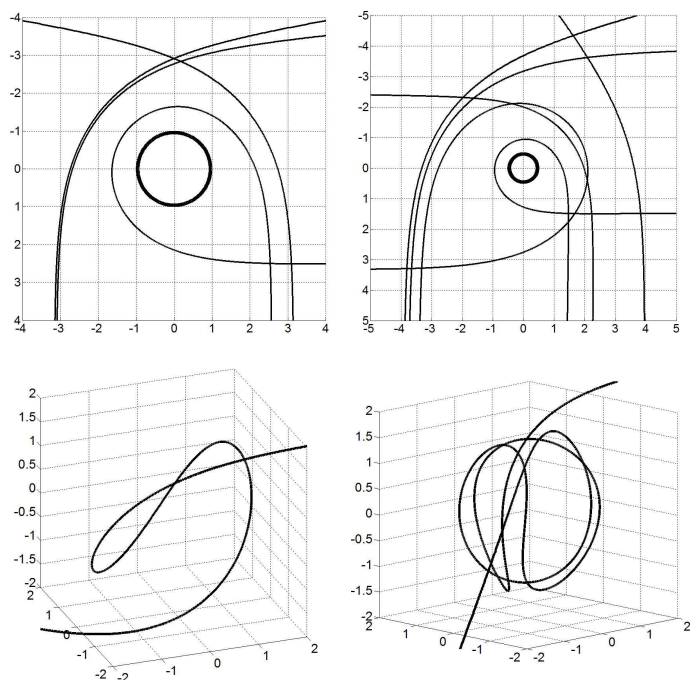


**Fig. 1.** Example of very long and complicated trajectories of the quantum in the Cartesian coordinate system. The black hole has extreme spin and it is placed at the point  $(0,0,0)$ . The top panels represent the flat trajectories. See the details in the text.

the spinning of the inertial frame), while the other one flies counter to the spinning.

In Kerr metric the trajectories can be very unusual and confusing, especially the non-flat trajectories. The bottom panels in Fig. 1 demonstrate two of these trajectories that make one and three revolutions around the black hole. All these complicated trajectories make the contribution to the image of the shadow and to the brightness of the thin annulus in the shadow area and should be taken into consideration. Thus, during the simulation process we have found the trajectory with 29 revolutions and a lot of trajectories with more than 5 revolutions.

## 5. Black hole shadows

### 5.1. Schwarzschild black hole

As it has already been mentioned that a shadow of a black hole is an area of the celestial sphere from which no one quanta arrives to the observer.

The shape of the shadow of the Schwarzschild black hole shown in Fig. 2. The top left panel represents the model where the standard screen is perpendicular to the line of view. The inner edge of the internal annulus should have the radius  $r = 3\sqrt{3}/2 \cdot r_g \approx 2.598 r_g$  (Zeldovich & Novikov 1964), that corresponds to the impact parameter at which the photon is captured by the black hole. Our numerical simulation confirms the fact that the internal radius of the annulus equals to  $2.598 r_g$  as well as the fact that the outer radius of the annulus is greater and equals to  $2.614 r_g$ . Between these values there is an infinite number of very thin annuli, corresponding to the increasing number of the revolutions of quantum with decreasing the impact radius from its largest value of  $2.614 r_g$  to the lowest one. It means that the thin annulus in the shadow in reality consists of a

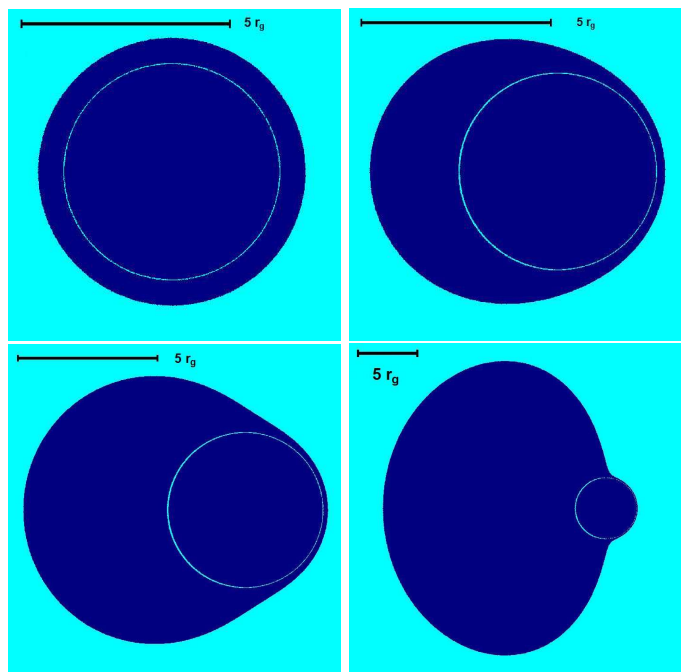


**Fig. 2.** Shadows of Schwarzschild black hole with different inclination angle of the standard screen. From top left panel to bottom right the angles are:  $0^\circ$ ,  $45^\circ$ ,  $60^\circ$  and  $81^\circ$ . The segments in the top left corners indicate the scale.

set of very thin rings and each of these thin rings includes the quanta that executes the same number of revolutions around the black hole. The outer radius of the shadow area is approximately  $3.084 r_g$ .

The top right panel in Fig. 2 demonstrates the shadow of the Schwarzschild black hole when the angle between the standard screen and the view line equals to  $45^\circ$ . The image here becomes asymmetrical and the shadow area increases. Nevertheless, the inner annulus has approximately the same size. This fact is clear from general physics because the annulus includes the quanta that make one or more revolutions around the black hole, so their impact parameter should be approximately unchanged.

The bottom panels in Fig. 2 presents the shadow of the black hole when the angle between the screen and the view line equals to  $60^\circ$  and  $81^\circ$ . The size of the shadow grows with increasing the inclination angle and at  $81^\circ$  its height becomes greater than its width whereas the size of the inner annulus remains essentially without changes.

### 5.2. Spinning black hole

The shape of the shadow of a spinning black hole (Kerr metric) is shown in Fig. 3. The Figure represents the geometry when both the standard screen and the spin axis are perpendicular to the view line. The horizontal shadow diameter is approximately  $6.11 r_g$ . The shadow shape is slightly asymmetrical and inside the shadow area we can see the thin annulus as it occurs in the Schwarzschild metric. But, unlike the Schwarzschild metric, the annulus is asymmetrical and its center does not coincide with the center of the shadow image. Moreover, one can distinguish a number of very thin rings on the right hand side of the inner annulus, but in the left side these rings are indistinguishable because the distance between them is very small. Each of these rings

refers to the quanta that executes a definite number of revolutions around the black hole (the quanta of the outer ring execute only one revolution).

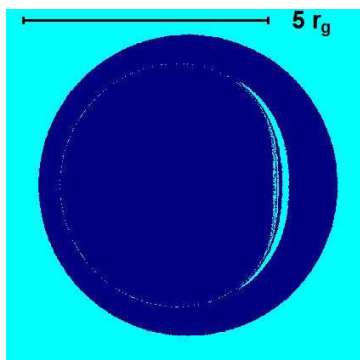


**Fig. 3.** Shadow of the spinning black hole. The view line is perpendicular to both the standard screen and the spin axis of the black hole. The segment at the top gives the scale. The shadow diameter (horizontal) is  $6.11 r_g$ .

The area inside the annulus is known as the shadow of a black hole under the assumption that the emission drops to the black hole from the solid angle  $4\pi$ . The edge of this area refers to the impact parameter at which the quantum drops into the black hole. The form of the shadows in this sense of the word is well known and it is presented in Chandrasekhar (1983) for marginally spinning black hole. This form coincides with that shown in Fig. 3.

## 6. Emission intensity

The form of the black hole shadow, presented in Figs. 2-3 is very interesting from a theoretical point of view. But for the observation carried out by space telescopes, the distribution of the emission intensity around and inside the shadow area is more important. This intensity is not a constant, of course.

To simulate the intensity distribution one should consider the so called „picture plane“, which is placed just in front of the observer. When we release a large amount of quanta in the direction of the black hole we distribute them uniformly in the tight solid angle and, consequently, they are distributed uniformly in the picture plane as well (the bright region in Figs. 2-3 has the uniform intensity). All these quanta, when they reach the standard screen, form there a non-uniform distribution. The emission of the standard screen is, however, uniform, according to the model. The idea is that we should find the continuous function which transforms the non-uniform distribution on the standard screen to the uniform one. Once found, this function gives us the possibility to assign each quantum a weight coefficient. If we then count all the quanta on the picture plane with their weight coefficients, we will have the true distribution of the emission intensity.

The distribution of the emission intensity for the marginally spinning black hole in the geometry where the view line is perpendicular to both the standard screen and the spinning axis is shown in Fig. 4. The  $y$ -axis is presented in the logarithmic scale and arbitrary (relative) units. The right panel demonstrates the distribution of the intensity in the equatorial plane. As it follows from the figure, the brightness of the image increases with decreasing the radial

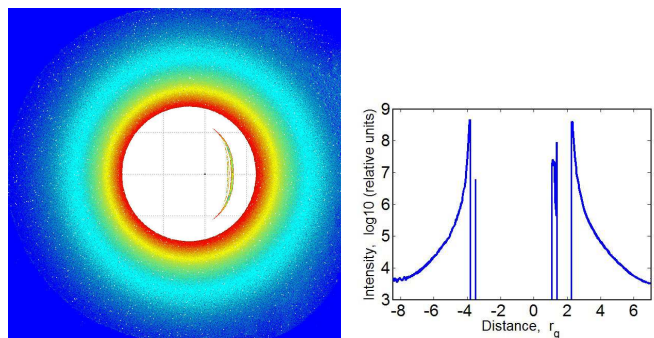


**Fig. 4.** Distribution of the emission intensity for the spinning black hole. The intensity is presented in conditional colors; the shadow area is white. The grid step is  $2r_g$ . The bold dot marks the center of the black hole. The right panel demonstrates the distribution of the intensity in the equatorial plane. The logarithmic scale is used along the  $y$ -axis.

coordinate and the increase covers more than four orders of magnitude. In reality, however, the intensity tends to infinity and the vertical line is the asymptote because the brightness of the optically thin standard screen becomes infinite at the edge. Except that, we consider in simulation the finite number of quanta and cannot obtain as a result the infinite intensity in principal. It means that the very top part of the curve may lay slightly higher than it is shown in the plot. The brightness of the inner annuli tends also to infinity at their edges.

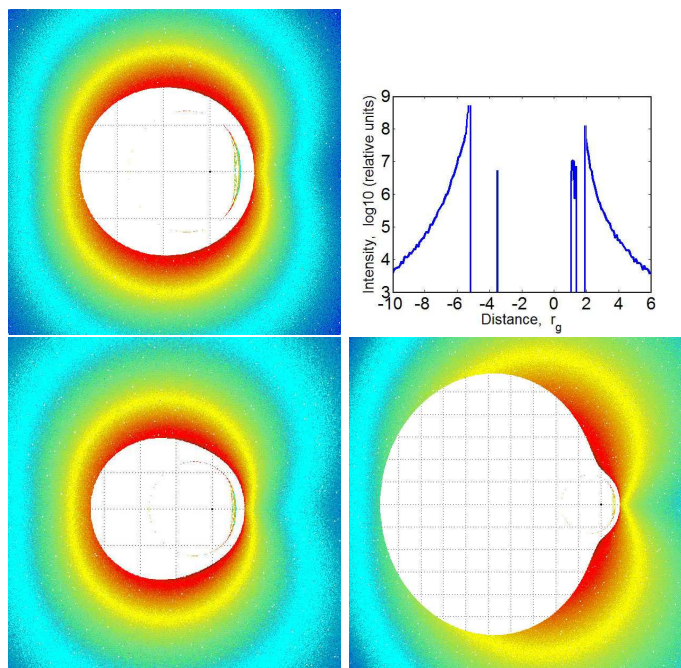


**Fig. 5.** Distribution of the emission intensity when the standard screen is on the left side of the observer. The intensity is presented in conditional colors; the shadow area is white. The grid step is  $2r_g$ . The images correspond to the angles of  $45^\circ$ ,  $60^\circ$  and  $80^\circ$  between the view line and the standard screen. The top right panel demonstrates the distribution of the intensity in the equatorial plane for the top left image.

The image of the shadow when the standard screen is not perpendicular to the view line is shown in Figs. 5-6. The images when the angle between the view line and the nor-



mal to the standard screen is positive presented in Fig. 5. Conditionally, one can say that the standard screen is located on the left hand side of the observer. The panels correspond to angles of  $45^\circ$ ,  $60^\circ$  and  $80^\circ$ . The distribution of the intensity in the equatorial plane for the angle of  $45^\circ$  is shown on the top right panel. This distribution differs from the one shown in Fig. 4, however the intensity at the edge of the shadow tends also to infinity.

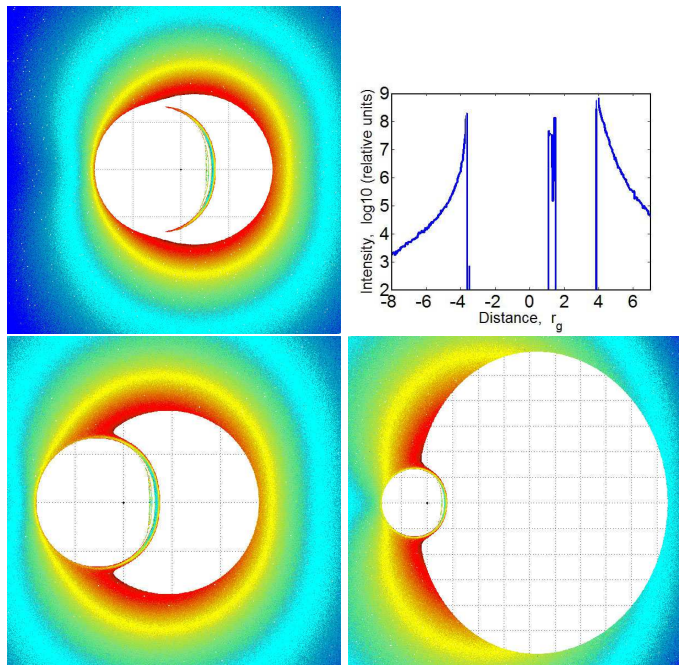


**Fig. 6.** Distribution of the emission intensity when the standard screen is on the left side of the observer. The intensity is presented in conditional colors; the shadow area is white. The grid step is  $2r_g$ . The images correspond to the angles of  $-45^\circ$ ,  $-60^\circ$  and  $-80^\circ$  between the view line and the standard screen. The top right panel demonstrates the distribution of the intensity in the equatorial plane for the top left image.

The images when the standard screen is to the right side from the observer, i.e. when the angle between the view line and the normal to the standard screen is negative is presented in Fig. 6. The panels correspond to the same angles between the view line and the normal to the standard screen and the top right panel also shows the intensity in the equatorial plane for the angle of  $45^\circ$ . The Figure differs significantly from its twin. The most interesting point is that the inner annulus here becomes bold and bright, however its form and size remain almost unchanged. Moreover, in the annulus we can distinguish even some very subtle individual rings. At the edges of the shadow the intensity tends to infinity.

If the standard screen is optically thick then the distribution of the emission intensity should differ from the optically thin case. Both distributions are presented in Fig. 7 for the case when the standard screen is perpendicular to the view line (the distribution for the optically thin case has already been presented in Fig. 4). As one can see, the difference between the two curves is so small that it becomes difficult to distinguish them by the naked eye. The right panel demonstrates this difference in the same scale. As it follows from the Figures the difference increases sharply and becomes significant only near the very edge of the shadow

(including the edges of the inner annuli). It means that the main contribution to the brightness of the ring around the shadow delivers very far areas of the standard screen.

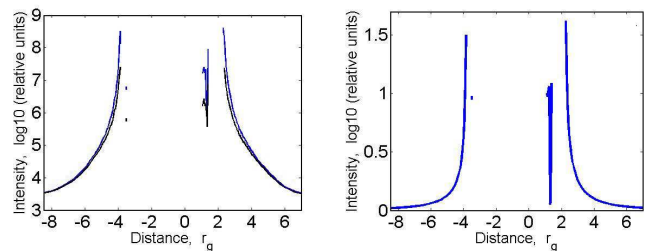


**Fig. 7.** Distribution of the emission intensity for optically thin and thick standard screen. One curve repeats the plot in Fig. 4 whereas the other one refers to the optically thick screen (the last curve lays lower). The right panel demonstrates the difference between the two cases in the same scale.

## 7. Discussion

The immediate observations of black holes are very important astrophysical problem, which is not solved yet. One possible solution is the attempt to observe the black hole shadow, which can be realized by the interferometer.

Even in the simplest formulation of the problem, which we consider, the shadow image appears rather complicated. It depends not only on the parameters of the black hole, but also on the characteristics of its surrounding. The real image can be extremely complicated, so the problem of the extraction of the parameters of the black hole becomes very difficult, if at all possible, to solve. Nevertheless, some peculiarities deliver us a hope that in some cases the problem can be formulated and solved. One of these cases is the characteristic distribution of the intensity around the shadow and the appearance of the internal arcs. In the nearest galaxies, such as M87, Andromeda and our Galaxy, the width of the arc inside the shadow area may reach 3-4 micro arc seconds. This detail is bright enough and probably can be registered in the observations.

We believe that it is important to separate the peculiarities of the shape of the shadow and distribution of the emission intensity related directly with the black hole from many complicated factors, such as the presence of the accreting disk with different distributions of the velocity and the temperature and so on. This separation is done in this paper.

## 8. Acknowledgements

One of the authors (S.R.) expresses his gratitude to Dr. O.Sumenkova, Dr. R.Beresneva and Dr. O.Kosareva for the opportunity for active and fruitful work on the problem.

The work has been partly supported by Grant of the President of the Russian Federation for Support of the Leading Scientific Schools NSh-6595.2016.2, grant RFBR No. 15-02-00554 and Basic Research Program P-7 of the Presidium of the Russian Academy of Sciences.

## References

Abdujabbarov, A., Amir, M., Ahmedov, B. and Ghosh, S.G. 2016, Phys. Rev. D **93**, 104004

- Akiyama, K., Lu, R.S., Fish, V.L. et al. 2015, ApJ, **807**, 150
- Amarilla, L., Eiroa, E.F. arXiv:1512.08956
- Bender R., Kormendy J., Bower G. et al. 2005, ApJ, **631**(1), 280, arXiv:astro-ph/0509839
- Broderick, A.E., Fish, V.L., Johnson, M.D. et al. 2016, ApJ, **820**, 137B, arXiv:1602.07701
- Carter, B. 1968, Phys. Rev. B, **174**, 1559
- Chandrasekhar, S. 1983, The mathematical theory of black holes. (Clarendon Press Oxford. Oxford University Press, New York).
- Cunha, P.V.P., Herdeiro, C.A.R., Radu, E., Runarsson, H.F. 2016, Int. J. of Mod. Phys. D, **25**(9), id. 1641021, arXiv:1605.08293
- Dexter, J., McKinney, J.C., Agol E. 2012, MNRAS, **421**, 1517
- Gear, C.W. 1971, Numerical Initial Value Problems in Ordinary Differential Equations. (Prentice Hall, Englewood Cliffs, NY)
- Ghasemi-Nodehi, M., Li, Z., Bambi, C. 2015, Eur.Phys.J. **C75**:315, arXiv:1506.02627
- Gillessen, S., Eisenhauer, F., Trippe, S. et al. 2009, ApJ, **692**, 1075.
- Johannsen, J., Broderick, A.E., Plewa, P.M. et al. 2016, Phys. Rev. Lett. **116**, 031101
- Kardashev, N.S., Novikov, I.D. Lukash, V.N. et al. 2014, Physics-Uspekhi, **57**(12), 1199
- Lacour, S., Eisenhauer, F., Gillessen, S. et al. 2014, A&A, **567**, A75
- Moscibrodzka, M., Falcke, H., Shiokawa, H. 2016, A&A, **586**, A38
- Neronov, A., Vovk, Ie. 2016, Phys. Rev. D, **93**(2), id.023006, arXiv:1506.08355
- Petzold, L.R. 1983, SIAM J. Sci. Stat. Comput. **4**, 136
- Shibley, J.O., Dolan, S.R. 2016, Class. Quant. Grav. **33**(17), 175001, arXiv:1603.04469
- Thorne K. 2014, The science of interstellar. (W.W.Norton & company, New York, London). ISBN 978-0-393-35137-8.
- Vincent, F.H. Paumard, T. Perrin, G. 2014, MNRAS, **441**(4), 3477
- Walsh, J.L., Barth, A.J., Ho, L.C., M. Sarzi, M. 2013, ApJ, **770**(2), 86, arXiv:1304.7273.
- Zakharov, A. F. 1994, MNRAS, **269**, 283.
- Zakharov, A. F. & Repin S. 1999, Astron. Reports, **43**, 705.
- Zakharov, A. F. & Repin S. 2002, Astron. Reports, **46**, 360.
- Zeldovich Ya.B., Novikov I.D. 1964, DAN USSR, **155**, 1033.